# Supplementary Materials: Broadband Terahertz Photonic Integrated Circuit with Integrated Active Photonic Devices

**Amlan kusum Mukherjee, Mingjun Xiang and Sascha Preu**

## 1. Details of the Experimental Setup

The homodyne photomixing setup, illustrated in Figure S1a) is composed of a source unit, consisting of a p-i-n diode-based commercial photomixer source from Toptica Photonics/Fraunhofer Heinrich Hertz institute, and a parabolic mirror for collimation of the THz beam. A TPX (Polymethylpentene) lens (L1) focuses the THz beam either into the waveguide (Figure S1b) or creates a focal point (Figure S1a). A second TPX lens (L2) collects and collimates the power emitted from the waveguide or passing through the intermediate focus. Finally, the beam propagates to the receiver unit, composed of a parabolic 90° off-axis mirror that focuses the THz beam onto a silicon-lens-coupled ErAs:InGaAs receiver ($Rx_{LP}$) with a logarithmic-periodic antenna [1]. Figure S1c shows a variant of the setup, where the receiver unit is replaced by the Vivaldi antenna for near field coupling directly from the waveguide without any free space optical components. The setup measures in the frequency domain by tuning the difference frequency of two continuous-wave lasers to the desired THz frequency. The p-i-n diode source mixes the two lasers, generating a THz beat note at the difference frequency that is emitted by an attached antenna. At the receiver side, the effect is reversed, mixing the beat note of the lasers with a received THz field in order to generate a DC current. Though the signals are measured in the frequency domain, a Fourier analysis enables switching to the time domain in order to remove undesired reflections in the setup, caused by imperfect components.

Both Tx and $Rx_{LP}$ are driven by two distributed feedback (DFB) lasers with a difference frequency in the terahertz range ($f_{THz}$). Tx is sinusoidally bias-modulated at 38.1 kHz by the Toptica source control unit. The $Rx_{LP}$ rectifies the received terahertz field and generates

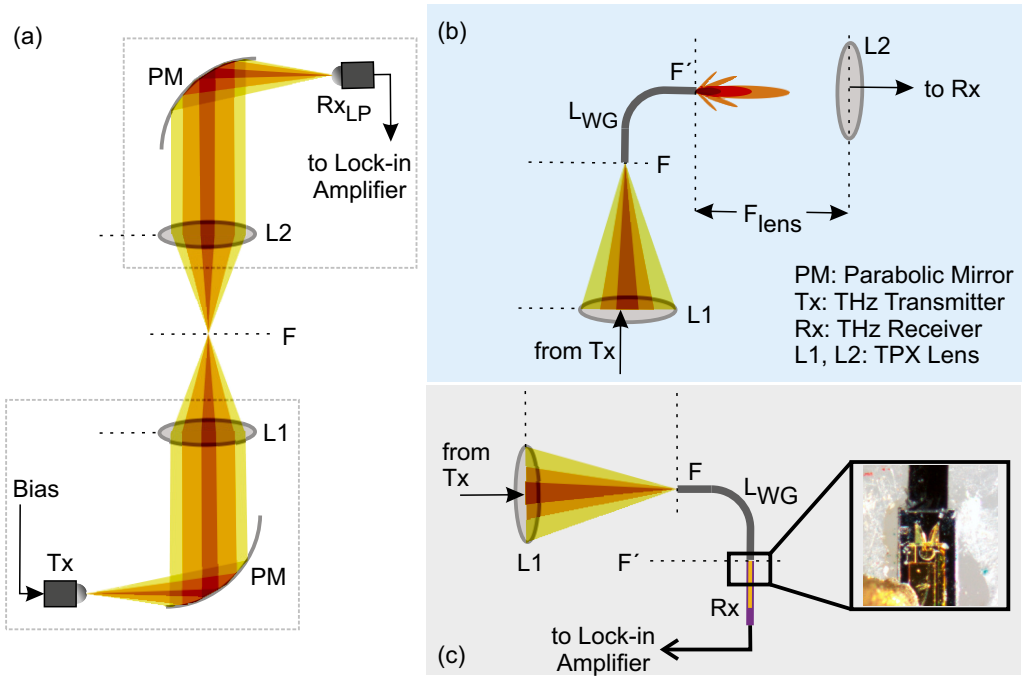


**Figure S1.** Experimental setup for free space measurements. (**a**) shows the reference measurement setup. Tx and Rx setups are modular, containing a parabolic mirror and a TPX lens each. (**b**) shows the setup for transmission measurement through a waveguide. The 90° bend prevents line-of-sight coupling from source to receiver. (**c**) setup with near field coupling, using a Vivaldi antenna.

a direct current (DC) proportional to the field of incident THz radiation. The generated DC is preamplified using a transimpedance amplifier (PDA-S from TEM Messtechnik) and then fed back to the Toptica source-control for lock-in detection. The measured current of the empty setup in Figure S1a) represents the reference detector current, $I_{ref}$. Then the waveguide is introduced into the setup as shown in Figure S1b) and $I_{WG}$, is recorded. Both currents are proportional to the THz field composed of the field amplitude and the relative phase between source and receiver arms [2]. The total loss in the system $L_{tot}$ (in decibels) calculates to

$$L_{tot,dB} = 20 \log_{10} \left( \left| \frac{I_{WG}}{I_{ref}} \right| \right). \quad (1)$$

The total loss is composed of coupling losses, guiding losses and material losses.

## 2. Conformal Transformation

The conformal transformation (Figure S2 a) transforms a circular waveguide (WG) bend (left) to an equivalent straight waveguide (right). The conformal transformed refractive index profile $n(\rho)$ of a bend with constant radius of curvature ($ROC$) becomes

$$n_t(u) = n\{\rho(u)\} \exp\left(\frac{u}{ROC}\right), \quad (2)$$

where $u = ROC \ln(\rho/ROC)$ is the transformed radial distance $\rho$. Radiative losses occur when the transformed permittivity of the surrounding media becomes higher than the effective permittivity of the guided mode at a certain distance to the waveguide $\rho_{lim}$ [3]. This results in a gradual radiation of the guided power carried in the evanescent field at $\rho > \rho_{lim}$, as illustrated in the main manuscript in Figure 3a and is also shown below in Figure S2b at $f_{THz} = 0.6$ THz. This radiative loss decreases with increasing frequency because the amount of power stored in the evanescent field decreases as well as with increasing $ROC$, which shifts $\rho_{lim}$ to larger values [4].

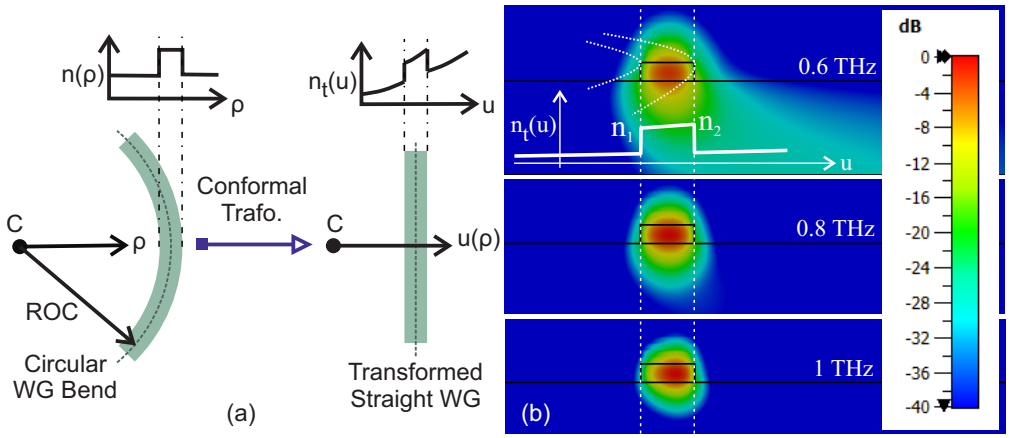


**Figure S2.** (a) Geometry and variable definitions of the conformal transformation. (b) shows the radiative losses and mode transformation at waveguide bends. The conformal-transformed refractive index $n_t(u)$ is plotted of a waveguide bend, with $ROC = 2$ mm where $n_1 = 3.25$ and $n_2 = 3.59$.

## 3. Calculation of Waveguide Dimensions

To estimate the dimensions of the HRFZ-Si waveguide analytically, we can approximate it as a slab waveguide (SWG) of height $h$, sandwiched by the same effective medium from top and bottom. For such a case, the fraction of half effective-wavelength along the vertical axis ($\lambda_y/2$) supported by SWG at any frequency ($f_{\mathrm{THz}}$) can be calculated by

$$m = \frac{h}{\lambda_y/2} = \frac{2hf_{THz}\sqrt{\epsilon_{r,Si} - \epsilon_{r,sur}}}{c_0}, \quad (3)$$

where $c_0$ is the speed of light in vacuum and $\epsilon_{r,sur}$ is the relative permittivity of the surrounding medium [5]. Since, the number of supported modes along the vertical axis is equal to the number of wave extrema along the same axis, a single-mode behaviour in SWG is only possible if $h < \lambda_y$, i.e., $m < 2$. Subsequently, by equating $h$ to the height of the rectangular HRFZ-Si waveguide, a single-mode operation over the whole operating frequency can be achieved by ensuring a single-mode behaviour at the highest operational frequency. For $m = 2$, $f_{\mathrm{THz}} = 2$ THz, $\epsilon_{r,Si} = 11.678$ and $\epsilon_{r,sur} \approx (\epsilon_{r,air} + \epsilon_{r,qz})/2 = 2.76$ in (3), the approximate height calculates to 50 $\mu$m. Similarly, $h$ is equated to the width of the designed waveguide such that it is single-mode at lowest operational frequency $f_{\mathrm{THz}} = 0.5$ THz, resulting in a width of $\approx$ 200 $\mu$m. These initial approximations are confirmed using simulations in CST Studio Suite and consequently, the design dimensions are set to $200 \times 50$ $\mu$m$^2$.

## 4. Simulation Results

### *4.1. In-Coupling Using Lenses*

For the presented waveguides, the source was in-coupled using a free space beam focused by a TPX lens on the end facet of a waveguide. The Gaussian spot diameter of the free-space THz beam at the foci of TPX lenses (F,F′) is $\approx$ 1300 $\mu$m at 0.5 THz and 1000 $\mu$m at 1 THz, i.e., more than an order of magnitude larger than the waveguide dimensions of $200 \times 50$ $\mu$m$^2$ which carries little field outside the waveguide at 1 THz, e.g., To improve the coupling in horizontal direction and increase the coupling efficiency, waveguides are tapered-out at the input and output apertures to $1000 \times 50$ $\mu$m$^2$.

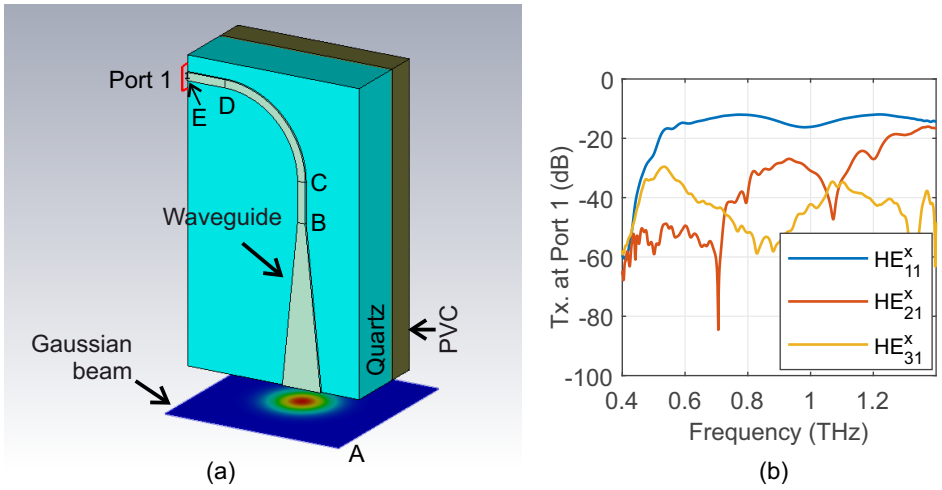


**Figure S3.** (a) shows the CST simulation model for the waveguide excited by a Gaussian beam. A waveguide port is placed at the end of the HRFZ-Si waveguide on a 520 $\mu$m thick quartz substrate, supported by PVC. Port 1 (outlined in red) absorbs all the power from the waveguide. Points A-E signify various location on the path of the propagating wave. (b) shows the simulated transmitted power to port 1 from the Gaussian beam for the first 3 horizontal modes in the waveguide.

Figure S3a shows the simulation model for this lens-assisted in-coupling scenario. Similar to the experimental setup, the silicon waveguide is placed on 520 $\mu$m thick quartz substrate, supported by a Polyvinyl Chloride layer to attenuate unguided power travelling in the substrate and from the incident Gaussian beam. The Gaussian-beam-field-source is placed 0.3 mm away from the waveguide facet at plane A, with appropriate beam diameter corresponding to the position. The waveguide is terminated using a waveguide port (Port 1) at point E. The ROC of the simulated bend is 2 mm and there are 0.5 mm long straight sections before (BC) and after (DE) the bend. The simulated transmitted power in the model is plotted in Figure S3b for the first three horizontal modes. Plots show that the transmitted power in fundamental mode is at least 15 dB larger than the higher order modes till $\sim$ 1.1 THz. Power coupled to HE$^x_{21}$ mode becomes significantly higher above

1.2 THz, becoming almost equal to that of the fundamental mode at $\sim$ 1.4 THz. Power coupled to other higher-order modes are weaker than $HE_{31}^{x}$ mode and hence, they do not significantly contribute to the total guided power.

Simulation of just the tapered in-coupling structure, along with the Gaussian excitation (section AC) shows a coupling efficiency of $-12$ to $-15$ dB for the fundamental mode. It can be thus inferred from plots in Figure S3b that coupling losses are the dominant loss mechanism as compared to material losses of straight waveguide sections or bend losses within the design range. Due to symmetry of the experimental setup, in- and out-coupling losses can be assumed equal and hence, a total loss between $24 - 30$ dB in the waveguide is expected. This is in line with the measurements of waveguides on quartz substrates that feature a total loss $L_{tot,dB}$ between $25 - 30$ dB. Reducing the dielectric permittivity of the substrate increases the mode field diameter as proven by placing the waveguide on HDPE, yet reducing the coupling losses by about 4 dB. Further improvement requires dedicated, broadband coupling structures as realized by the Vivaldi antenna near field couplers.

### *4.2. Mode Conversion in Waveguide Bends*

Four waveguide bends with radii of curvature (*ROC*) 1, 2, 3 and 4 mm are simulated using CST microwave studio. An input waveguide port is placed at location B in Figure S3a and sections preceding B are discarded. The input port is only excited in the fundamental mode and S21 parameters at the output port at E is measured for first three horizontal modes for bends with different *ROC*s. The total length of the waveguide (BE) is kept constant. Plots in Figure S4 show the power coupled to fundamental and higher order modes after the waveguide bends.

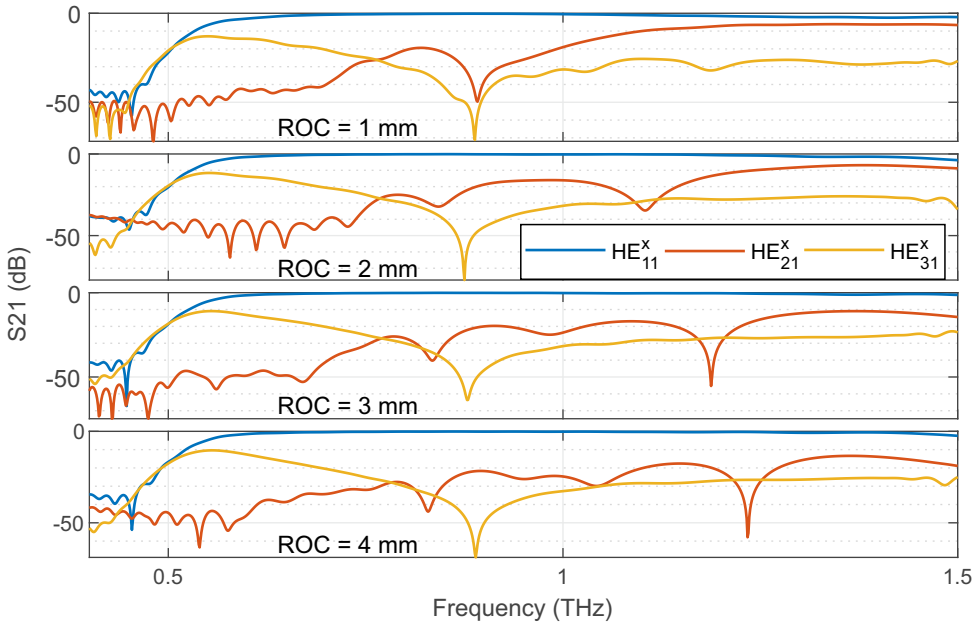


**Figure S4.** Plots show simulated higher order mode generation at waveguide bends for different radius of curvatures between 1 and 4 mm.

Two inferences can be drawn from the simulated transmission characteristics of the bends. First, the power converted to $HE_{31}^{x}$ in the bends above 0.6 THz is $< -20$ dB. We see similar features in Figure 4a, where the measured bend losses stagnates after 0.6 THz. Secondly, as *ROC*s increase, the power coupled to $HE_{21}^{x}$ mode significantly decreases at higher frequencies above 1 THz. For a bend radius of $\leq 2$ mm, significant mode conversion occurs above $\sim$ 1.1 THz, which is also evident in Figure 7a and Figure S3b. $ROC \geq 4$ mm can further diminish mode conversions at the bends, even till 1.5 THz.

It is to be noted that cyanoacrylate adhesive between the waveguide and quartz substrate is not considered in these simulations as it only increases the propagation losses,

without having any apparent effect on mode conversion. It is, however, possible that at lower frequencies, where the guided wave is loosely bound to the waveguide, geometric imperfections in the guiding structure can generate additional radiation modes, which leads to excess power loss [6]. This results in increased discrepancies between the simulated attenuation coefficient and the measured value in Figure 2b at lower frequencies.

**5. Distinction between Higher Order Modes and Standing Waves**

The waveguides are measured in a homodyne setup, i.e., the transmitter and the receiver are driven by the same set of lasers, where the measured receiver current is proportional in the incident Terahertz electric field at the receiver [7] multiplied by the cosine of phase difference incident field and the beating frequency of the lasers at the receiver. The detector current reads as,

$$I_{Rx}(f) = kE_{THz}(f)\cos\left(\frac{\omega\Delta d}{c_0}\right) = \frac{1}{2}kE_{THz}(f)\left[\exp\left(-j\frac{\omega\Delta d}{c_0}\right) + \exp\left(j\frac{\omega\Delta d}{c_0}\right)\right], \quad (4)$$

where $E_{THz}$ is the magnitude of the incident electric field on the receiver, $k$ is a constant, $\omega = 2\pi f$ is the angular frequency, $c_0$ is the speed of light in vacuum and $2\pi f/c_0\Delta d$ is the phase difference between the laser signal at the transmitter and the receiver caused by a path length difference of $\Delta d$. Using inverse Fourier transform, the corresponding time domain signal $i_{Rx}(t)$ can be written as,

$$\mathfrak{F}^{-1}[I_{Rx}(f)] = i_{Rx}(t) = \frac{k}{2}\left[e_{THz}(t-t_0) + e_{THz}(t+t_0)\right], \quad (5)$$

where $t_0 = \Delta d/c_0$. The second term in eqn. (5) can be ignored due to its non-causality. Thus, the time domain signal $i_{Rx}(t)$ represents the received terahertz pulse at the receiver at the delay of $t_0$. This delay $t_0$ can be further written as a sum of free-space delay $t_{FS}$ and waveguide delay $t_{WG}$ components as,

$$t_0 = t_{FS} + t_{WG} = t_{FS} + \frac{l_{WG}}{c_0/\sqrt{\epsilon_{r,eff}}}, \quad (6)$$

where $l_{WG}$ is the length of the waveguide and $\epsilon_{r,eff}$ is the relative effective permittivity of the propagating mode. Since $\epsilon_{r,eff}$ of the fundamental mode is highest among all other modes, the power travelling in higher order modes (HOMs) will have a smaller delay than that of the power travelling in the fundamental mode, i.e., they will arrive at the receiver before the fundamental mode. On the other hand, standing waves (SW) are generated by the echoes of the propagating mode due to the reflections at the waveguide end-facets. These echoes will reach the receiver at a greater delay than the fundamental mode.

Table 1: Waveguide parameters plotted in Figure S5.

| **Notation** | **W1** | **W2** | **W3** | **W4** |
|---|---|---|---|---|
| **Length (mm)** | $19.14 \pm 0.5$ | $19.14 \pm 0.5$ | $22.71 \pm 0.5$ | $19.14 \pm 0.5$ |
| **ROC (mm)** | 1.0 | 2.0 | 3.0 | 4.0 |
| $t_{0,FM}$ **(ns)** | 2.435 | 2.426 | 2.464 | 2.426 |

Plots in Figure S5 show the time domain plots for a reference signal in Figure S5a as well as the signal through the waveguides tabulated in Table 1. The dispersive nature of the waveguide is clear from the transmission characteristics, as the pulse is significantly broadened during transmission. Figure S5b and d shows initial measurements of W1 and W2, respectively. Additional peaks before the main peak, i.e., at a delay $< 2.43$ ns, are present which indicate the generation of higher order modes. All waveguides with $ROC = 1$ mm have this feature, indicating inevitable mode conversion at the waveguide

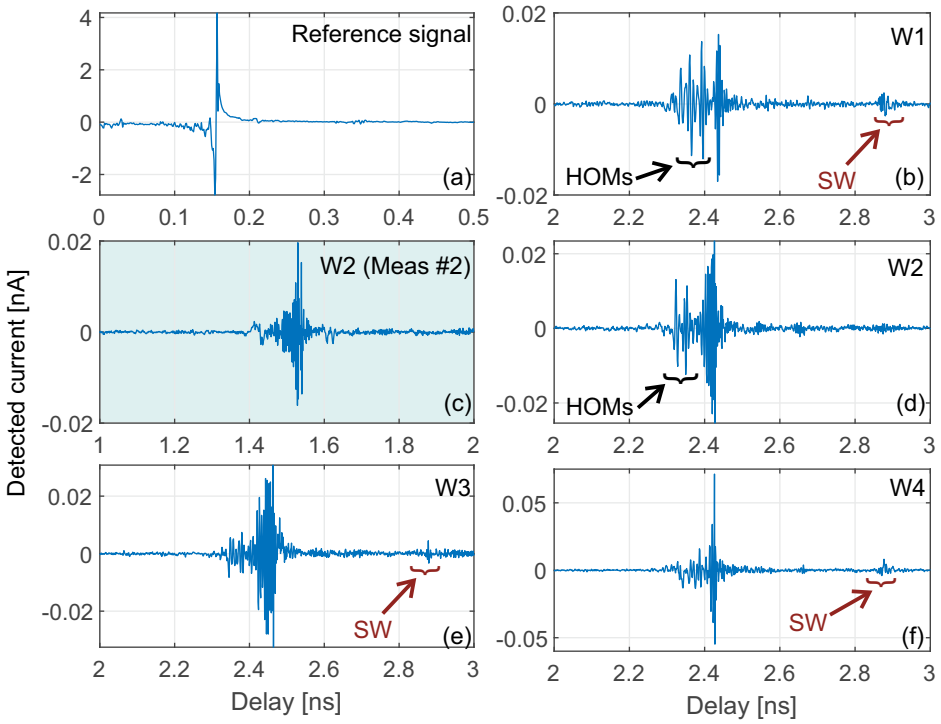


**Figure S5.** (a) shows a the reference signal in time-domain (b)-(f) show time domain signal of the measured transmission trough the waveguides. Fig. (a)-(b) and (d)-(f) are measured in the same setup, whereas (c) is measured in a different setup (altered optical fibre of the receiver) and hence the main peak delay is smaller than the other plots.

bend. However, a remeasurement of W2 depicted in S5c) shows an insignificant higher order mode generation due to a better alignment of the waveguide. For higher *ROC*s, the generated higher order mode is significantly lower than the power in the fundamental mode. However, smaller copies of the signal can be seen arriving at the receiver after the main peak, indicating presence of standing waves in the measurements.

An optical path length difference of 11.4 mm can be ascertained from the excess delay of the main peak of W3 ($l_{WG} = 22.71$ mm) with respect to W2 ($l_{WG} = 19.14$ mm) in Table 1, which corresponds to an effective refractive index of $3.19 \pm 0.4$ ($7.67 < \epsilon_{r,eff} < 12.74$) considering the measurement error of the waveguide lengths. This value is slightly higher than the simulated permittivity values, which is probably due to the presence of superglue underneath the waveguides. We note that both the effects of higher order modes and standing waves can be reduced by filtering the frequency domain signal using a bandpass filter (equivalent to windowing in time domain).

## 6. Whispering Gallery Mode Resonator atop Waveguides

The power coupled in whispering gallery mode (WGM) resonators placed adjacent to the waveguides is low due to the lack of evanescent field outside the waveguides along its width at higher frequencies. However, if the resonator is placed on top of the waveguides, similar to configurations showed by Vogt et al. [8], higher coupling efficiencies can be achieved. Figure S6a shows the simulation schematic, where a 180 $\mu$m thick WGM resonator with 1 mm diameter is directly placed on the HRFZ-Si waveguide supported by a HDPE substrate. Figure S6b shows the simulated $S_{21}$ parameter of such a resonator configuration in dB. Resonance features with $< -20$ dB transmission can be observed even at frequencies as high as 1.2 THz. However, we note that we will need to used adhesive to directly mount the resonator structure on the waveguide, which will add losses to the structures, eventually leading to a lower quality factor of the resonance peaks.

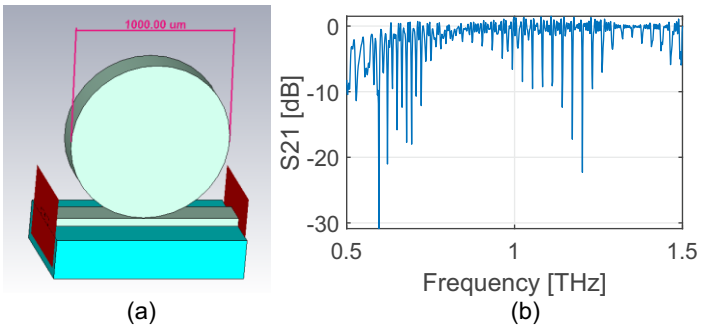


**Figure S6.** (a) Model of a WGM resonator placed on top of the HRFZ-Si waveguide (b) shows simulated transmission characteristics of such a resonator configuration.

## References


1. Olvera, A.F.; Lu, H.; Gossard, A.C.; Preu, S. Continuous-wave 1550 nm operated terahertz system using ErAs:In(Al)GaAs photo-conductors with 52 dB dynamic range at 1 THz. *Opt. Express* **2017**, *25*, 29492–29500. doi:10.1364/OE.25.029492.
2. Preu, S.; Döhler, G.H.; Malzer, S.; Wang, L.J.; Gossard, A.C. Tunable, continuous-wave Terahertz photomixer sources and applications. *Journal of Applied Physics* **2011**, *109*, 061301, [https://doi.org/10.1063/1.3552291]. doi:10.1063/1.3552291.
3. Heiblum, M.; Harris, J. Analysis of curved optical waveguides by conformal transformation. *IEEE Journal of Quantum Electronics* **1975**, *11*, 75–83. doi:10.1109/JQE.1975.1068563.
4. Marcatili, E.A.J. Bends in Optical Dielectric Guides. *Bell System Technical Journal* **1969**, *48*, 2103–2132. doi:10.1002/j.1538-7305.1969.tb01167.x.
5. Marcatili, E.A.J. Dielectric rectangular waveguide and directional coupler for integrated optics. *The Bell System Technical Journal* **1969**, *48*, 2071–2102. doi:10.1002/j.1538-7305.1969.tb01166.x.
6. Yeh, C.; Shimabukuro, F.I., Propagation Characteristics of Guided Waves Along a Dielectric Guide. In *The Essence of Dielectric Waveguides*; Springer US: Boston, MA, 2008; pp. 55–98. doi:10.1007/978-0-387-49799-0_3.
7. Preu, S.; Döhler, G.H.; Malzer, S.; Wang, L.J.; Gossard, A.C. Tunable, continuous-wave Terahertz photomixer sources and applications. *Journal of Applied Physics* **2011**, *109*, 061301, [https://doi.org/10.1063/1.3552291]. doi:10.1063/1.3552291.
8. Vogt, D.W.; Leonhardt, R. Ultra-high Q terahertz whispering-gallery modes in a silicon resonator. *APL Photonics* **2018**, *3*, 051702, [https://doi.org/10.1063/1.5010364]. doi:10.1063/1.5010364.